# Structure and Dynamics of Peptide−Amphiphiles Incorporating Triple-Helical Proteinlike Molecular Architecture†

Ying-Ching Yu,[‡,§] Vikram Roontga,[||,⊥] Vladimir A. Daragan,[||] Kevin H. Mayo,[||] Matthew Tirrell,[§] and Gregg B. Fields*[,‡,▽]

*Departments of Laboratory Medicine & Pathology, Chemical Engineering & Materials Science, and Biochemistry, University of Minnesota, Minneapolis, Minnesota 55455, and Department of Chemistry & Biochemistry and the Center for Molecular Biology & Biotechnology, Florida Atlantic University, Boca Raton, Florida 33431-0991*

*Received September 25, 1998; Revised Manuscript Received December 3, 1998*

ABSTRACT: Organized polymeric assemblies that incorporate bioactive sequences and structures are finding important applications for the study of protein structure−function relationships. We have recently described a heteropolymeric peptide−amphiphile system that forms organized structures in solution and on surfaces. While the overall three-dimensional features of peptide−amphiphiles have been studied previously, the precise environment of specific residues, particularly those within biologically active regions, have not been examined in detail. In the present study, we have used heteronuclear single quantum coherence (HSQC) and inverse-detected $^{1}H-^{15}N$ NMR spectroscopy to examine the structure and dynamics of a peptide and peptide−amphiphile that incorporate the α1(IV)1263−1277 ([IV-H1]) amino acid sequence from type IV collagen. Three variants of the sequence $(Gly\text{-}Pro\text{-}Hyp)_4$-[IV-H1]-$(Gly\text{-}Pro\text{-}Hyp)_4$ were constructed with a single $^{15}N$-labeled Gly placed in the middle of the *N*-terminal $(Gly\text{-}Pro\text{-}Hyp)_4$ region (residue $Gly^{7}$), in the middle of the [IV-H1] sequence (residue $Gly^{19}$), or in the middle of the *C*-terminal $(Gly\text{-}Pro\text{-}Hyp)_4$ region (residue $Gly^{34}$). These peptides were also *N*-terminally acylated with hexanoic acid to create an analogous series of $^{15}N$-labeled peptide−amphiphiles. HSQC spectra indicated that both the peptide and the peptide−amphiphile were in triple-helical conformation at low temperature, supporting prior circular dichroism (CD) spectroscopic results. The intensities of the triple-helical cross-peaks were stronger for the peptide−amphiphile, consistent with an enhanced triple-helical thermal stability within the peptide−amphiphile construct compared to that of the peptide alone. Relative relaxation values for the peptide−amphiphile monomeric and trimeric species were consistent with those reported previously for other triple-helical peptides. Relaxation measurements indicated that the triple-helical [IV-H1] region did not appear to be dramatically more flexible than the Gly-Pro-Hyp regions. The angle between Gly N−H bonds and the helix dyad axis, determined from the relaxation data, was within the range expected for triple helices. Overall, the peptide headgroup of the $C_6$-$(Gly\text{-}Pro\text{-}Hyp)_4$-[IV-H1]-$(Gly\text{-}Pro\text{-}Hyp)_4$ peptide−amphiphile appears to form a continuous triple helix that behaves similarly, in a dynamic sense, to a triple-helical peptide. The enhanced thermal stability of the peptide−amphiphile compared to the analogous triple-helical peptide, along with the multitude of organized structures formed by lipidlike compounds, suggest that peptide−amphiphiles could be utilized as targeted liposomes, sensors, receptors, or enzymes.

The design of organized polymeric assemblies that incorporate bioactive sequences and/or structures represents a burgeoning area of biochemical and biomaterials research. Such polymers have been developed for modulation of protein−ligand interactions (*1*), protein adsorption to surfaces (*2*), and cell adhesion (*3*−*6*). We have recently described a heteropolymeric peptide−amphiphile system that forms organized structures in solution and on surfaces (*7*−*10*). The peptide−amphiphile has a peptide "headgroup", which contains a bioactive sequence and has the propensity to form secondary, supersecondary, and/or tertiary structures, and a lipophilic "tail", which is composed of mono- or dialkyl hydrocarbon chains. In principle, the lipophilic tail regions will associate by hydrophobic interactions, inducing and/or stabilizing the three-dimensional structure of the peptide headgroup. Our initial studies have indeed demonstrated that triple-helical and α-helical protein-like molecular architecture is stabilized in the peptide−amphiphile (*8*−*11*). Other groups have also found induction of peptide structure by lipophilic

† This research is supported from the Center for Interfacial Engineering (NSF CDR-8721551), University of Minnesota MRSEC, Earl E. Bakken Chair for Biomedical Engineering, and NIH (CA77402, HL62427, and AR 01929). G.B.F. is a recipient of an NIH RCDA.

* To whom correspondence should be addressed at the Department of Chemistry & Biochemistry, Florida Atlantic University, 777 Glades Rd., Boca Raton, FL 33431-0991. Phone 561-297-2093; Fax 561-297-2759; E-mail fieldsg@fau.edu.

‡ Department of Laboratory Medicine & Pathology, University of Minnesota.

§ Department of Chemical Engineering & Materials Science, University of Minnesota.

|| Department of Biochemistry, University of Minnesota.

⊥ Present address: Pharmaceutical Research Institute, Bristol-Myers Squibb, Princeton, NJ 08540.

▽ Florida Atlantic University.

10.1021/bi982315l CCC: $18.00 
Published on Web 01/14/1999

compounds. For example, when the peptide acetyl-Lys-Gly-Arg-Gly-Asp-Gly amide is attached to dodecylphosphocholine, the peptide−amphiphile forms a type II or I′ turn conformation, while the peptide itself mixed with the phopholipid does not (*12*). *N*-Octadecanoyl $(Gly)_n$ ethyl ester monolayers and Langmuir−Blodgett films, where $n = 1-5$, form polyGly II helices while the oligoGly peptides do not (*13*). The next stage in the evolution of synthetic peptide−amphiphiles is the detailed three-dimensional structural analysis of both the peptide headgroup and the lipophilic tail, as well as a more comprehensive understanding of the forces responsible for inducing the respective structures of these components.

Our peptide−amphiphile system has utilized headgroups that have primarily been based on collagen triple-helical structural elements (*8*−*11*). The triple helix consists of three polypeptide chains, each in an extended, left-handed polyPro II-like helix, which are staggered by one residue and then supercoiled along a common axis in a right-handed manner (*14*). Geometric constraints of the triple-helical structure require that every third amino acid is Gly, resulting in a Gly-X-Y repeating sequence. The X and Y positions are commonly occupied by imino acids, with the triplet Gly-Pro-Hyp known to be the strongest promoter of triple-helical conformation (*14*). Substantial stabilization of the triple-helical structure can be achieved with the introduction of a di-Lys or di-Glu template at the *C*- or *N*-terminal regions of the three peptide chains (*14*−*19*), a double disulfide "knot" at the *C*-terminal region of the three peptide strands (*20*), or a Kemp triacid template linked to the *N*-terminus of three peptide chains (*21*−*23*). Conversely, we have described the noncovalent, peptide−amphiphile self-assembly approach to building a collagenlike structural motif (*8*, *9*). The thermal stability of the triple-helical headgroup can be controlled by the lipophilic tail length and extent of branching (*8*, *10*, *11*). This is especially important for the function of bioactive sequences, where the maintenance of distinct three-dimensional structure may correlate to optimal activity (*15*). In some cases, fluctuations in the triple-helical backbone are possible (*24*, *25*) and may be necessary for some collagen-mediated activities (*26*).

The potential activities mediated by triple helices are quite varied. Collagen's triple-helical conformation can modulate cell and platelet binding (*15*, *16*, *27*, *28*) and induction of signaling pathways (*29*). The triple helix is found in a variety of proteins in addition to collagen, such as macrophage scavenger receptors types I and II and bacteria-binding receptor MARCO, complement component C1q, pulmonary surfactant apoprotein, acetylcholinesterase, and mannose binding protein (*14*, *30*). Triple-helical conformation appears to have an important role in the binding of acetylated low-density lipoprotein (Ac-LDL) (*17*, *31*) and tetraplex nucleic acids (*32*) to macrophage scavenger receptor type I.

In the present and prior studies, we have incorporated a type IV collagen-derived cell adhesion site ([IV-H1])[1] into peptide−amphiphiles. The bioactive collagen sequence is then flanked by Gly-Pro-Hyp repeats (*8*, *9*, *11*). The [IV-H1] sequence, Gly-Val-Lys-Gly-Asp-Lys-Gly-Asn-Pro-Gly-Trp-Pro-Gly-Ala-Pro from α1(IV)1263−1277, is known to promote melanoma cell adhesion and spreading (*33*−*35*). Triple-helical conformation greatly enhances the biological activity of [IV-H1] (*9*, *10*, *35*). The [IV-H1] sequence alone forms a distinct, non-triple-helical structure in solution with unique backbone and side-chain mobilities (*34*, *36*−*38*). One is particularly concerned as to the structure of the [IV-H1] sequence within the peptide−amphiphile, i.e., does the sequence itself form a triple helix or are only the surrounding Gly-Pro-Hyp regions in triple-helical conformation. Flexibility of triple-helical structure may have subtle effects on biological recognition processes (*26*). In our prior studies, triple-helical structure of the peptide−amphiphiles was confirmed by circular dichroism (CD) spectroscopy and two-dimensional NMR spectroscopy of the Pro and Hyp side chains within and/or surrounding the [IV-H1] site (*8*, *11*). The present work employs NMR spectroscopy to further characterize the peptide−amphiphile and the [IV-H1] sequence itself.

High-resolution multidimensional NMR has been successfully applied to structural and dynamic studies of many biomolecules. The study of protein structure by NMR spectroscopy relies on the observation of NOEs and spin−spin coupling constants $^3J_{HN\alpha}$. NOEs occur between two atoms at distances smaller than 5 Å. The $^3J_{HN\alpha}$ coupling constants depend on dihedral angles. The distance constraints derived from NOEs and dihedral angle constraints may then be used for creating computer models of the protein. Difficulties arise when these approaches are used to determine the structure of a triple helix. The three strands in a triple helix are staggered by one residue and often of the same sequence. When NOEs are observed, it is difficult to distinguish between interchain and intrachain NOEs since both are within 5 Å, and one would anticipate both intra- and interchain NOEs for triple helices (*39*−*42*). Even when nonsequential NOEs may exist, it is very difficult to assign the cross-peaks due to severe overlapping (*40*−*42*). One approach has been to compare observed NOEs of backbone protons with those predicted by models for triple-helical structure based on X-ray analyses of collagen and model peptides (*39*). However, with $^{15}N$ or $^{13}C$ residues, it is possible to study specific regions within collagenous peptides (*41*, *43*). In the present study, we have used site-specific $^{15}N$-labeled peptides and peptide−amphiphiles in concert with two-dimensional NMR spectroscopy to (1) provide further evidence that monoalkyl peptide−amphiphiles are in triple-helical conformation, (2) examine the dynamics of monoalkyl peptide−amphiphiles, and (3) investigate the [IV-H1] region to see if a biologically active sequence within a peptide−amphiphile is in triple-helical conformation.

## EXPERIMENTAL PROCEDURES

*Synthesis of Peptides and Peptide−Amphiphiles.* All standard peptide synthesis chemicals and solvents were analytical reagent grade or better and were purchased from

[1] Abbreviations: CD, circular dichroism; DIEA, *N*,*N*-diisopropylethylamine; Fmoc, 9-fluorenylmethoxycarbonyl; HBTU, *N*-[(1*H*-benzotriazol-1-yl)(dimethylamino)methylene]-*N*-methylmethanaminium hexafluorophosphate *N*-oxide; HMQC, heteronuclear multiple quantum coherence; HOBt, 1-hydroxybenzotriazole; HSQC, heteronuclear single quantum coherence; Hyp, 4-hydroxy-L-proline; [IV-H1], Gly-Val-Lys-Gly-Asp-Lys-Gly-Asn-Pro-Gly-Trp-Pro-Gly-Ala-Pro; MALDI-TOF-MS, matrix-assisted laser desorption/ionization time-of-flight mass spectrometry; NMR, nuclear magnetic resonance; RP-HPLC, reversed-phase high performance liquid chromatography; TFA, trifluoroacetic acid.

Perkin-Elmer/Applied Biosystems Division (Foster City, CA) or Fisher Scientific (Pittsburgh, PA). Fmoc-4-[[(2′,4′-dimethoxyphenyl)amino]methyl]phenoxy resin (substitution level = 0.46 mmol/g) was purchased from Novabiochem (La Jolla, CA). All Fmoc-amino acid derivatives were from Novabiochem and are of L-configuration. HOBt was purchased from Novabiochem, HBTU from Quantum Biotechnologies (Montreal, Quebec), DIEA from Fisher Scientific, hexanoic acid [$CH_3$-$(CH_2)_4$-$CO_2H$, designated $C_6$] from Aldrich, and Fmoc-$^{15}$N-Gly from Cambridge Isotope Laboratories (Andover, MA).

Peptide−resin assembly was performed by Fmoc solid-phase methodology on an ABI 431A peptide synthesizer (*44*) with appropriate modifications (*16*, *45*). All peptides and peptide−amphiphiles were synthesized as C-terminal amides to prevent diketopiperazine formation. Peptide−resins were characterized by Edman degradation sequence analysis as described previously for "embedded" (noncovalent) sequencing (46). Peptide−resins were then either (a) cleaved or (b) lipidated with the $C_6$ tail (*8*) and then cleaved. Cleavage and side-chain deprotection of peptide−resins and peptide−amphiphile−resins proceeded for 2 h with 1,2-ethanedithiol−thioanisole−phenol−$H_2O$−TFA (2.5:5:5:5:82.5) as described (*47*). Peptide−amphiphile cleavage solutions were extracted with methyl *t*Bu ether prior to purification.

*Peptide Purification and Analysis.* Preparative RP-HPLC purification was performed on a Rainin AutoPrep System. Peptides were purified with a Vydac 218TP152022 $C_{18}$ column (15−20 $\mu$m particle size, 300 Å pore size, 250 × 25 mm) at a flow rate of 5.0 mL/min. The elution gradient was either 0−60% buffer B or 0−100% buffer B in 60 min, where buffer A was 0.1% TFA in $H_2O$ and buffer B was 0.1% TFA in acetonitrile. Detection was at 280 nm. Peptide−amphiphile purification was achieved on a Vydac 214TP152022 $C_4$ column (15−20 $\mu$m particle size, 300 Å pore size, 250 × 22 mm) at a flow rate of 5.0 mL/min. The elution gradient was 30−100% buffer B in 70 min where buffer A was 0.05% TFA in $H_2O$ and buffer B was 0.05% TFA in 2-propanol. Detection was at 280 nm. Analytical RP-HPLC was performed on a Hewlett-Packard 1090 liquid chromatograph equipped with a Hypersil $C_{18}$ column (5 $\mu$m particle size, 120 Å pore size, 200 × 2.1 mm) at a flow rate of 0.3 mL/min. The elution gradient was 0−60% buffer B in 45 min where buffers A and B were the same as for peptide purification. Diode array detection was at 220, 254, and 280 nm.

Edman degradation sequence analysis was performed on an Applied Biosystems 477A protein sequencer/120A analyzer. MALDI-TOF-MS was performed on a Hewlett-Packard G2025A LD-TOF mass spectrometer with a sinapinic acid matrix (*7*, *8*). All peptides gave the desired sequence, and all peptides and peptide−amphiphiles had proper mass values.

*NMR Spectroscopy.* NMR spectra were acquired on a 600 MHz Varian INOVA spectrometer. Freeze-dried samples for NMR spectroscopy were dissolved in $D_2O$ or $D_2O$−$H_2O$ (1:9) at peptide and peptide−amphiphile concentrations of 3−5 mM at least 48 h prior to experiments. Two-dimensional sensitivity-enhanced HSQC spectroscopy (*48*) experiments were recorded at 25 and 45 °C with 256 *t*1 increments. The spectral widths were 7200 Hz in the *t*2 dimension and 2000 Hz in the *t*1 dimension. $^{15}$N $T_1$, $T_2$, and heteronuclear NOE were measured in experiments with "reverse" proton detection (*48*, *49*). For the peptide−amphiphiles with $^{15}$N-labeled Gly in the *N*-terminal (Gly-Pro-Hyp)$_4$ or in the *C*-terminal (Gly-Pro-Hyp)$_4$, one-dimensional versions of the pulse sequences were used since the signals in the HSQC spectra do not overlap in the *t*2 dimension. A spectral width of 7200 Hz was used in the *t*2 dimension, and a spectra width of 2000 Hz was used in the *t*1 dimension. For the $T_1$ and $T_2$ experiments, 32 scans per *t*1 increment were accumulated. For the NOE experiment, 128 scans per *t*1 increment were recorded. $T_1$ values were obtained with relaxation delays of 5.5, 71.5, 159.5, 269.5, 401.5, 577.5, and 836.0 ms. $T_2$ values were measured with delays of 16, 32, 48, 64, 80, 113, and 145 ms. For measuring $^1$H−$^{15}$N NOE, spectra were recorded in the presence and absence of $^1$H saturation. $^{15}$N $T_1$, $T_2$, and heteronuclear NOE values were calculated as described previously (*24*).

*Motional Models for Analysis of NMR Relaxation Data.* The general equation for the rotational correlation function for motions of some vector $\boldsymbol{a}$ can be written as (*50*)

$$C_a(t) = 4\pi\langle Y_{20}[\theta_a(t)]Y_{20}[\theta_a(0)]\rangle \quad (1)$$

and for the Lipari−Szabo model-free approach (*51*, *52*)

$$C_a(t) = \exp(-t/\tau_0)[S_a^2 + (1 - S_a^2)\exp(-t/\tau_i)] \quad (2)$$

where $\tau_0$ is the correlation time for overall tumbling, $\tau_i$ is the correlation time for internal motion, and $S_a^2$ is an order parameter that reflects incomplete motional averaging of the bond vector within a particular molecular frame. In general, $S_a^2$ is the limiting value of the internal correlation function at $t \rightarrow \infty$:

$$S_a^2 = 0.8\pi \sum_{m=-2}^{2} \langle Y_{2m}(\theta_a,\varphi_a)\rangle\langle Y^*_{2m}(\theta_a,\varphi_a)\rangle \quad (3)$$

$\theta_a$ and $\varphi_a$ are polar angles defining the motional vector $\boldsymbol{a}$ in the molecular frame.

For molecules that are nonspherical in shape, such as collagen triple helices, the Lipari−Szabo approach does not provide an accurate model for deriving motional parameters since it does not consider the influence of rotational anisotropy. The anisotropy of overall tumbling prevents factorization of the correlation function as shown in eq 2, even when internal bond rotations and overall molecular tumbling occur independently. To address this, one can consider the symmetric top rotational diffusion model (*50*) parametrized with diffusion coefficients $D_\parallel$ and $D_\perp$. The diffusive frame $\{X_D, Y_D, Z_D\}$ can be chosen such that the $Z_D$ axis is directed along the $D_\parallel$ rotational axis. Having transformed the laboratory frame into the diffusive frame, the correlation function can be written as

$$C_a(t) = 0.8\pi \sum_{q=-2}^{2} \langle D^*_{0q}{}^{(2)}[\Omega_{LD}(t)]\, D_{0q'}{}^{(2)}[\Omega_{LD}(0)]\, Y_{2q}[a_D(t)]\, Y^*_{2q}[a_D(0)]\rangle \quad (4)$$

$\Omega_{LD}(t)$ are Euler angles for transformation from the laboratory frame to the molecular (diffusive) frame. $a_D(t)$ denotes the orientation of the motional vector $\boldsymbol{a}$ in the diffusive frame. If one assumes that internal bond rotations and overall

tumbling occur independently for rotational diffusion of the symmetric top, one can write

$$\langle D^*_{0q}{}^{(2)}[\Omega_{LD}(t)]D_{0q'}{}^{(2)}[\Omega_{LD}(0)]\rangle = 0.2\delta_{qq'}\exp(-D_q t) \quad (5)$$

where

$$D_q = 6D_\perp + (D_\parallel - D_\perp)q^2 \quad (6)$$

By use of Euler angles $\{0, \beta, \gamma_0 + \gamma(t)\}$ for the second transformation from the diffusive frame to the $\{X_R, Y_R, Z_R\}$ frame wherein the $Z_R$ axis is directed along the average orientation of vector ***a***, a general equation for the correlation function can be obtained:

$$C_a(t) = 0.8\pi \sum_{q,m,m'} e^{-Dqt}\, d_{qm}{}^{(2)}(\beta)\, d_{qm'}{}^{(2)}(\beta)\, C_{mm'}(t) \quad (7)$$

$$C_{mm'}(t) = \langle Y_{2m}[\theta_a(t),\varphi_a(t)]Y^*_{2m'}[\theta_a(0),\varphi_a(0)]\rangle \quad (8)$$

$q$, $m$, $m'$ are equal to $-2$, $-1$, 0, 1, 2. $d_{qm}{}^{(2)}(\beta)$ terms are reduced Wigner functions. $\beta$ is the angle formed between $Z_D$ and $Z_R$ axes, and $\theta_a$ and $\varphi_a$ are polar angles that define motional vector ***a*** within the $\{X_R, Y_R, Z_R\}$ molecular frame. If one now assumes that vector ***a*** wobbles about its equilibrium position within a cone having semiangle $\theta_0$, the limiting value of the correlation function $C_{mm'}(t)$ can be expressed as

$$C_{mm'}(\infty) = S^2\delta_{m0}\delta_{m'0} \quad (9)$$

where

$$S^2 = 0.25\cos^2\theta_0(1 + \cos\theta_0)^2 \quad (10)$$

Since backbone atoms within the triple helix structure are probably motionally restricted, one may further assume that the decay of the internal motional correlation function is very fast and that the amplitude of the wobbling motion is small. In this case, the spectral density, $J_a(\omega)$, which corresponds to the correlation function given by eq 7, can be written as

$$J_a(\omega) = S^2[P_2{}^2(\cos\beta)J_0(\omega) + 3\cos^2\beta\sin^2\beta\, J_1(\omega) + 0.75\sin^4\beta J_2(\omega)] \quad (11)$$

where

$$J_q(\omega) = D_q/(D_q{}^2 + \omega^2) \quad (12)$$

## RESULTS AND DISCUSSION

*Conformation of Peptides and Peptide−Amphiphiles.* A vast number of approaches have been described by which proteinlike molecular architecture can be created and stabilized. We have recently examined the use of lipophilic compounds for potentially aligning peptide strands and inducing and/or stabilizing proteinlike secondary, supersecondary, and tertiary structures within these peptide sequences (*7*−*9*). Our initial studies demonstrated that dialkyl ester compounds of carbon chain lengths 12−18 stabilize triple-helical conformation (*8*, *9*). We have subsequently shown that monoalkyl carbon chains of lengths 6−16 also stabilize triple-helical conformation (*10*, *11*). Specifically,

**(A)** (Gly-Pro-Hyp)$_4$-[IV-H1]-(Gly-Pro-Hyp)$_4$-$NH_2$

**(B)** $CH_3$-$(CH_2)_4$-C(=O)-(Gly-Pro-Hyp)$_4$-[IV-H1]-(Gly-Pro-Hyp)$_4$-$NH_2$

**(C)**
Gly-Pro-Hyp-Gly-Pro-Hyp-**Gly**-Pro-Hyp-Gly-Pro-Hyp
Gly-Pro-Hyp-Gly-Pro-Hyp-**Gly**-Pro-Hyp-Gly-Pro-Hyp
Gly-Pro-Hyp-Gly-Pro-Hyp-**Gly**-Pro-Hyp-Gly-Pro-Hyp

**(D)**
Gly-Val-Lys-Gly-Asp-Lys-**Gly**-Asn-Pro-Gly-Trp-Pro-Gly-Ala-Pro
Gly-Val-Lys-Gly-Asp-Lys-**Gly**-Asn-Pro-Gly-Trp-Pro-Gly-Ala-Pro
Gly-Val-Lys-Gly-Asp-Lys-**Gly**-Asn-Pro-Gly-Trp-Pro-Gly-Ala-Pro

FIGURE 1: General sequences of the $^{15}$N-labeled (A) peptides and (B) peptide−amphiphiles used for HSQC experiments. The proper triple-helical alignments of the (C) (Gly-Pro-Hyp)$_4$ *N*- or *C*-terminal regions and (D) [IV-H1] region are shown.

CD and one-dimensional NMR spectroscopic studies of the peptide−amphiphile $C_6$-(Gly-Pro-Hyp)$_4$-[IV-H1]-(Gly-Pro-Hyp)$_4$ indicated that a short monoalkyl chain exerts a significant stabilizing effect on proteinlike structure.

To further study the structure and dynamic properties of triple-helical peptides and peptide−amphiphiles, site-specific $^{15}$N-labeled peptides were synthesized. Three variants of (Gly-Pro-Hyp)$_4$-[IV-H1]-(Gly-Pro-Hyp)$_4$ were constructed, each with a single $^{15}$N-labeled Gly. The $^{15}$N-labeled amino acid was placed in the middle of the *N*-terminal (Gly-Pro-Hyp)$_4$ region (residue Gly$^7$), the middle of the [IV-H1] sequence (residue Gly$^{19}$), or the middle of the *C*-terminal (Gly-Pro-Hyp)$_4$ region (residue Gly$^{34}$) (Figure 1). These peptides were also acylated with a $C_6$ tail to create an analogous series of $^{15}$N-labeled peptide−amphiphiles. Studies of these biomolecules proceeded by heteronuclear $^1$H−$^{15}$N correlation NMR spectroscopy.

HSQC experiments were performed initially on labeled (Gly-Pro-Hyp)$_4$-[IV-H1]-(Gly-Pro-Hyp)$_4$ (Figure 2). We first examined the peptide containing $^{15}$N-Gly$^7$ (Figure 2, left panel). The HSQC spectrum at 25 °C shows two major cross-peaks occurring at 7.86 and 8.38 ppm. The 8.38 ppm cross-peak is accompanied by a cross-peak at 8.32 ppm. The intensity of the cross-peak at 7.86 ppm is much weaker than the intensity of the 8.38 ppm cross-peak. A very similar spectrum is obtained for the peptide containing $^{15}$N-Gly$^{34}$ at 25 °C (Figure 2, right panel). However, the peptide containing $^{15}$N-Gly$^{19}$ has a very different HSQC spectrum at 25 °C (Figure 2, center panel). Four cross-peaks are found, occurring at 8.26, 8.32, 8.45, and 8.48 ppm. The cross-peaks at 8.32, 8.45, and 8.48 ppm are of equal intensity. The 8.26 ppm cross-peak is accompanied by a cross-peak at 8.19 ppm.

HSQC experiments were next performed for (Gly-Pro-Hyp)$_4$-[IV-H1]-(Gly-Pro-Hyp)$_4$ at 45 °C (Figure 3). Since (Gly-Pro-Hyp)$_4$-[IV-H1]-(Gly-Pro-Hyp)$_4$ has a melting temperature ($T_m$) of 35.6 °C (*8*), NMR data obtained at 45 °C will be indicative of the monomeric (non-triple-helical) peptide. The spectrum of [$^{15}$N-Gly$^7$]-(Gly-Pro-Hyp)$_4$-[IV-H1]-(Gly-Pro-Hyp)$_4$ (Figure 3, left panel) shows one major and one minor cross-peak. The cross-peak found at 7.86 ppm in the 25 °C spectrum has disappeared, while the 8.38 ppm cross-peak has shifted upfield to ∼8.18 ppm. In similar fashion, the spectrum of [$^{15}$N-Gly$^{34}$]-(Gly-Pro-Hyp)$_4$-[IV-H1]-(Gly-Pro-Hyp)$_4$ (Figure 3, right panel) shows one major and one minor cross-peak. The cross-peak found at 7.86 ppm in the 25 °C spectrum has disappeared, while the 8.38 ppm cross-peak has shifted to ∼8.18 ppm. The spectrum of the

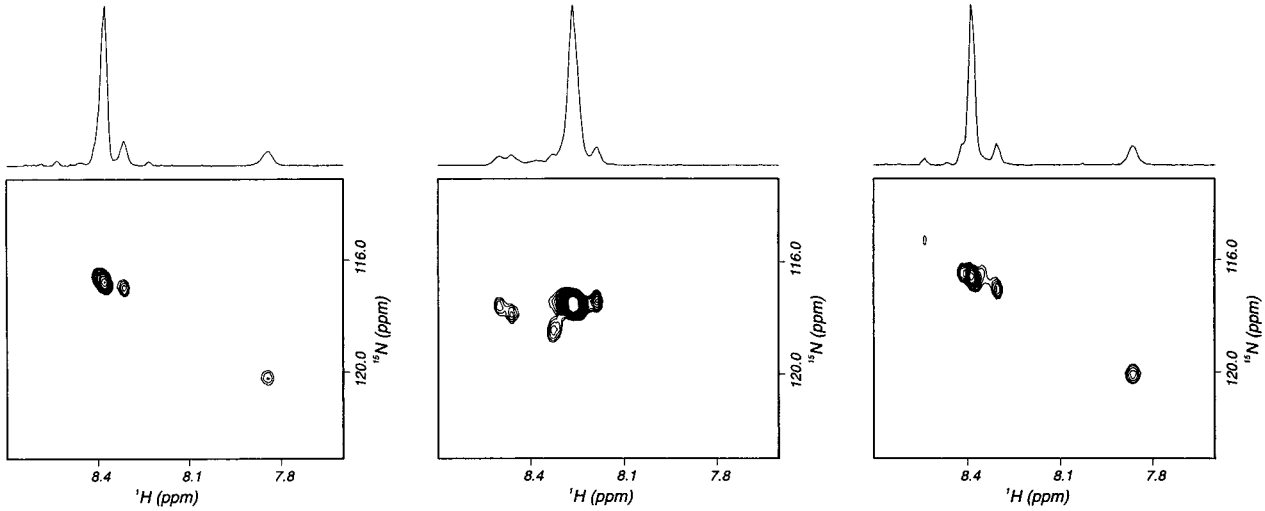


FIGURE 2: HSQC spectra for (left panel) [$^{15}$N-Gly$^7$]-(Gly-Pro-Hyp)$_4$-[IV-H1]-(Gly-Pro-Hyp)$_4$, (center panel) [$^{15}$N-Gly$^{19}$]-(Gly-Pro-Hyp)$_4$-[IV-H1]-(Gly-Pro-Hyp)$_4$, and (right panel) [$^{15}$N-Gly$^{34}$]-(Gly-Pro-Hyp)$_4$-[IV-H1]-(Gly-Pro-Hyp)$_4$ at 25 °C. Two major cross-peaks occurring at 7.86 and 8.38 ppm are found for the peptide containing $^{15}$N-Gly$^7$ or $^{15}$N-Gly$^{34}$. The peptide containing $^{15}$N-Gly$^{19}$ exhibits four cross-peaks occurring at 8.26, 8.32, 8.45, and 8.48 ppm. Conditions are given in Experimental Procedures.

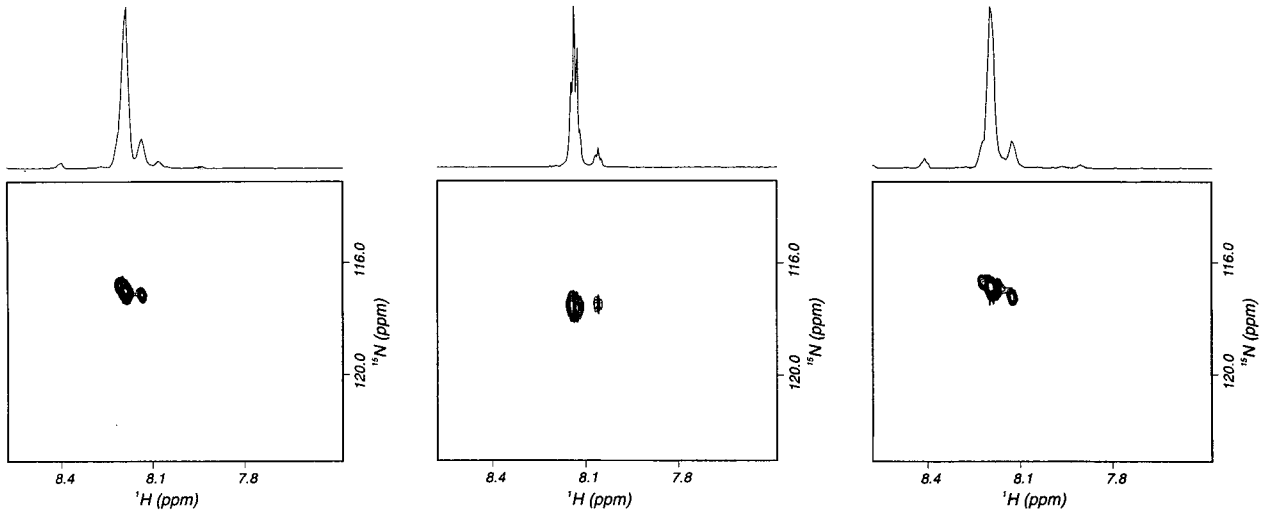


FIGURE 3: HSQC spectra for (left panel) [$^{15}$N-Gly$^7$]-(Gly-Pro-Hyp)$_4$-[IV-H1]-(Gly-Pro-Hyp)$_4$, (center panel) [$^{15}$N-Gly$^{19}$]-(Gly-Pro-Hyp)$_4$-[IV-H1]-(Gly-Pro-Hyp)$_4$, and (right panel) [$^{15}$N-Gly$^{34}$]-(Gly-Pro-Hyp)$_4$-[IV-H1]-(Gly-Pro-Hyp)$_4$ at 45 °C. One major cross-peak occurring at 8.18 ppm is found for the peptide containing $^{15}$N-Gly$^7$, $^{15}$N-Gly$^{19}$, or $^{15}$N-Gly$^{34}$. Conditions are given in Experimental Procedures.

peptide containing $^{15}$N-Gly$^{19}$ (Figure 3, middle panel) is now similar to those of the $^{15}$N-Gly$^7$ and $^{15}$N-Gly$^{34}$ peptides, in that only one major and one minor cross-peak is seen. The three cross-peaks occurring at 8.32, 8.45, and 8.48 ppm in the 25 °C spectrum have disappeared, and the 8.26 ppm cross-peak has shifted to ∼8.18 ppm. The transition of the peptide (Gly-Pro-Hyp)$_4$-[IV-H1]-(Gly-Pro-Hyp)$_4$ from a triple-helical state at 25 °C to a monomeric, non-triple-helical state at 45 °C results in significant changes in the HSQC spectra.

HSQC experiments were repeated with the C$_6$-(Gly-Pro-Hyp)$_4$-[IV-H1]-(Gly-Pro-Hyp)$_4$ peptide−amphiphile. At 25 °C, the spectrum of the peptide−amphiphile containing $^{15}$N-Gly$^7$ (Figure 4, left panel) shows two major cross-peaks occurring at 7.86 and 8.38 ppm, in fashion similar to the peptide. However, unlike the peptide spectrum (Figure 2, left panel), the intensity of the cross-peak at 7.86 ppm is stronger than the intensity of the 8.38 ppm cross-peak. A very similar spectrum is obtained for the peptide−amphiphile containing $^{15}$N-Gly$^{34}$ at 25 °C (Figure 4, right panel). The 25 °C HSQC spectrum of the peptide−amphiphile containing $^{15}$N-Gly$^{19}$ has four cross-peaks occurring at 8.26, 8.32, 8.45, and 8.48 ppm (Figure 4, center panel). The intensities of the 8.32, 8.45, and 8.48 ppm cross-peaks are equivalent to each other and greater for the peptide−amphiphile than for the peptide alone at 25 °C (see Figure 2, center panel).

HSQC experiments were performed for C$_6$-(Gly-Pro-Hyp)$_4$-[IV-H1]-(Gly-Pro-Hyp)$_4$ at 45 °C (Figure 5). Since C$_6$-(Gly-Pro-Hyp)$_4$-[IV-H1]-(Gly-Pro-Hyp)$_4$ has a $T_m$ of 42.2 °C (10), NMR data obtained at 45 °C will be indicative primarily of the monomeric (non-triple-helical) peptide−amphiphile. The spectrum of [$^{15}$N-Gly$^7$]-C$_6$-(Gly-Pro-Hyp)$_4$-[IV-H1]-(Gly-Pro-Hyp)$_4$ (Figure 5, left panel) shows one major and one minor cross-peak. The cross-peak found at 7.86 ppm in the 25 °C spectrum has disappeared, while the 8.38 ppm cross-peak has shifted to ∼8.18 ppm. In similar fashion, the spectrum of [$^{15}$N-Gly$^{34}$]-C$_6$-(Gly-Pro-Hyp)$_4$-[IV-H1]-(Gly-Pro-Hyp)$_4$ (Figure 5, right panel) shows one major and one minor cross-peak. The cross-peak found at 7.86 ppm in the 25 °C spectrum has disappeared, while the 8.38 ppm cross-peak has shifted to ∼8.18 ppm. The spectrum of the peptide−amphiphile containing $^{15}$N-Gly$^{19}$ (Figure 5, middle panel) is now similar to $^{15}$N-Gly$^7$ and $^{15}$N-Gly$^{34}$, in that only

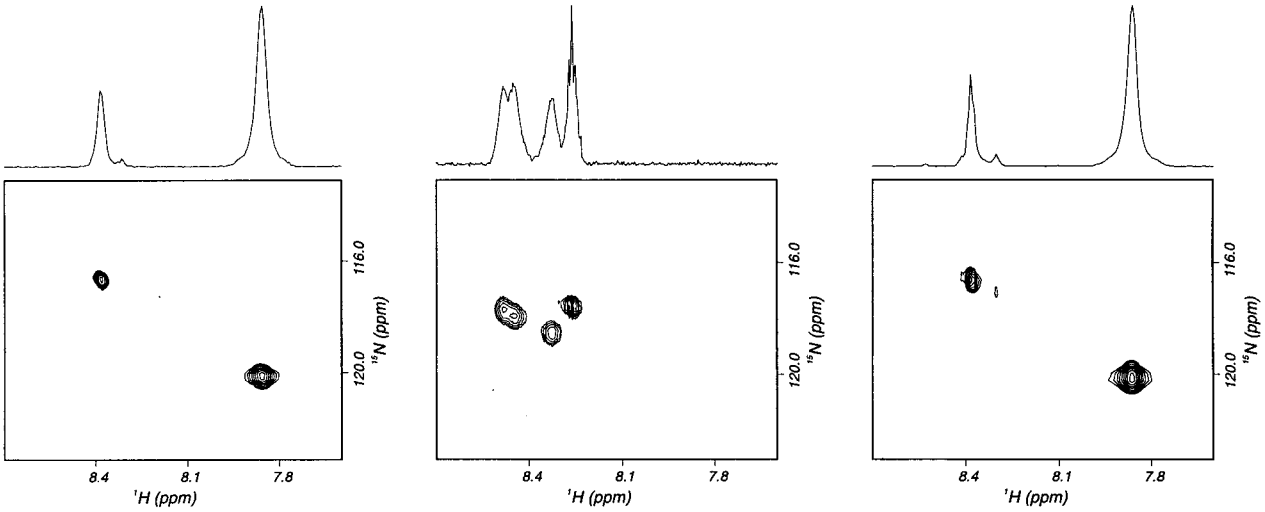


FIGURE 4: HSQC spectra for (left panel) [$^{15}$N-Gly$^7$]-$C_6$-(Gly-Pro-Hyp)$_4$-[IV-H1]-(Gly-Pro-Hyp)$_4$, (center panel) [$^{15}$N-Gly$^{19}$]-$C_6$-(Gly-Pro-Hyp)$_4$-[IV-H1]-(Gly-Pro-Hyp)$_4$, and (right panel) [$^{15}$N-Gly$^{34}$]-$C_6$-(Gly-Pro-Hyp)$_4$-[IV-H1]-(Gly-Pro-Hyp)$_4$ at 25 °C. Two major cross-peaks occurring at 7.86 and 8.38 ppm are found for the peptide−amphiphile containing $^{15}$N-Gly$^7$ or $^{15}$N-Gly$^{34}$. The peptide−amphiphile containing $^{15}$N-Gly$^{19}$ exhibits four cross-peaks occurring at 8.26, 8.32, 8.45, and 8.48 ppm. Conditions are given in Experimental Procedures.

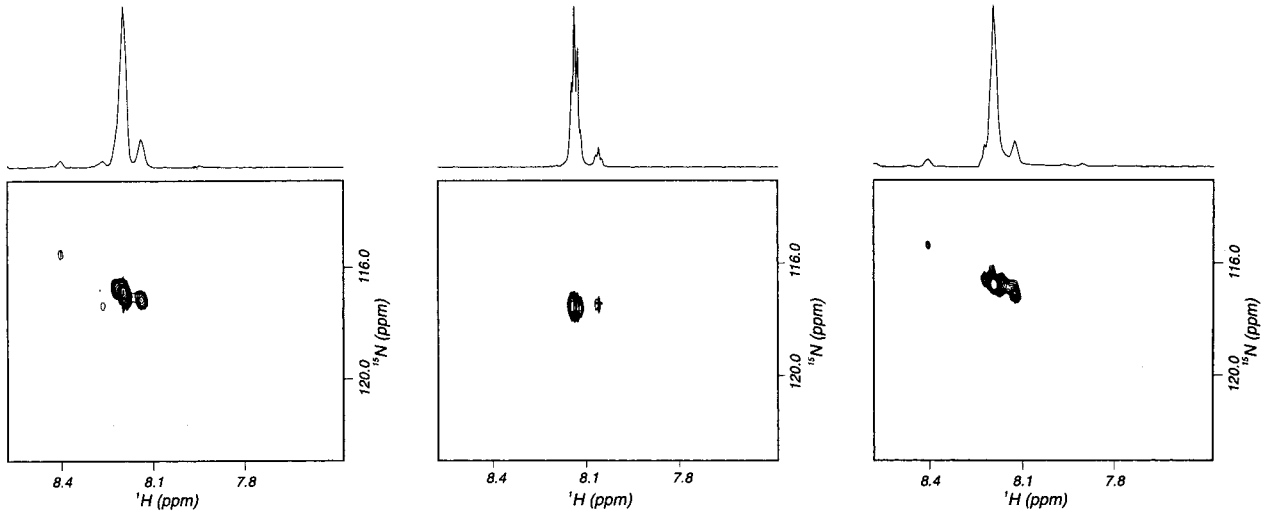


FIGURE 5: HSQC spectra for (left panel) [$^{15}$N-Gly$^7$]-$C_6$-(Gly-Pro-Hyp)$_4$-[IV-H1]-(Gly-Pro-Hyp)$_4$, (center panel) [$^{15}$N-Gly$^{19}$]-$C_6$-(Gly-Pro-Hyp)$_4$-[IV-H1]-(Gly-Pro-Hyp)$_4$, and (right panel) [$^{15}$N-Gly$^{34}$]-$C_6$-(Gly-Pro-Hyp)$_4$-[IV-H1]-(Gly-Pro-Hyp)$_4$ at 45 °C. One major cross-peak occurring at 8.18 ppm is found for the peptide−amphiphile containing $^{15}$N-Gly$^7$, $^{15}$N-Gly$^{19}$, or $^{15}$N-Gly$^{34}$. Conditions are given in Experimental Procedures.

one major and one minor cross-peak are seen. The three cross-peaks occurring at 8.32, 8.45, and 8.48 ppm in the 25 °C spectrum have disappeared, and the 8.26 ppm cross-peak has shifted to ∼8.18 ppm. The transition of the peptide−amphiphile $C_6$-(Gly-Pro-Hyp)$_4$-[IV-H1]-(Gly-Pro-Hyp)$_4$ from a triple-helical state at 25 °C to a monomeric, non-triple-helical state at 45 °C results in significant changes in the HSQC spectra, in fashion similar to those seen for the peptide alone.

HSQC spectra of the peptide and peptide−amphiphile containing $^{15}$N-Gly$^{19}$ showed four cross-peaks at 25 °C, three of which disappeared at 45 °C. These three cross-peaks could correspond to individual peptide strands in triple-helical conformation. Since the three strands in a triple helix are staggered by one residue, the $^{15}$N-Gly$^{19}$ in each peptide chain of the triple-helical peptide or peptide−amphiphile would be in a different environment with respect to neighboring residues (*14*, *41*) (see Figure 1). Thus, the three $^{15}$N-Gly$^{19}$ residues would have different chemical shifts if a properly aligned triple-helix was formed. In addition, the intensities of the three cross-peaks should be similar. Our results are consistent with these assumptions, and thus the [IV-H1] region within both the peptide and peptide−amphiphile appears to be in triple-helical conformation. The various cross-peaks can be assigned to a triple-helical or monomeric state (Table 1).

Other researchers have previously documented similar two-dimensional NMR spectral behavior for diverse sequence triple-helical peptides. One example is peptide T3-785, which incorporates α1(III) collagen residues 785−796 (*39*). HSQC spectra of [$^{15}$N-Ala$^{13}$]-T3-785 showed four Ala-related cross-peaks, three of which disappeared with increasing temperature (*53*). HMQC spectra of [$^{15}N_3$-Gly$^{15}$,Leu$^{16}$,Ala$^{17}$]-T3-785 showed 12 cross-peaks for the three labeled residues, nine of which disappeared above the melting temperature of the triple-helical peptide (*24*). A second example is MSR-1, a peptide derived from the collagenous domain of macrophage scavenger receptor (*54*). HSQC spectra of [$^{15}$N-Gly$^{15}$]-MSR-1 showed four cross-peaks, three of which disappeared with increasing temperature (*54*). If in proper

Table 1: $^{15}$N and $^{1}$H Chemical Shifts for (Gly-Pro-Hyp)$_4$-[IV-H1]-(Gly-Pro-Hyp)$_4$ and $C_6$-(Gly-Pro-Hyp)$_4$-[IV-H1]-(Gly-Pro-Hyp)$_4$[a]

| $^{15}$N-labeled residue | conformational state | (N)$^{1}$H (ppm) | $^{15}$N(H) (ppm) |
|---|---|---|---|
| $Gly^7$ | monomeric | 8.38 | 110.2 |
| $Gly^7$ | trimeric | 7.86 | 106.6 |
| $Gly^{19}$ | monomeric | 8.26 | 109.2 |
| $Gly^{19}$ | trimeric | 8.48 | 109.2 |
| $Gly^{19}$ | trimeric | 8.45 | 108.9 |
| $Gly^{19}$ | trimeric | 8.32 | 108.4 |
| $Gly^{34}$ | monomeric | 8.38 | 110.2 |
| $Gly^{34}$ | trimeric | 7.86 | 106.6 |

[a] $^{1}$H chemical shifts are expressed relative to sodium 3-(trimethylsilyl)tetradeuteriopriopionate. $^{15}$N chemical shifts are expressed relative to liquid $NH_3$.

register, four cross-peaks per $^{15}$N-labeled residue within a diverse triple-helical sequence have been demonstrated. Three cross-peaks are assigned to the triple-helical conformation, while one corresponds to the monomeric (non-triple-helical) state.

In contrast to the [IV-H1] region, the $^{15}$N-labeled Gly residues in the middle of a (Gly-Pro-Hyp)$_4$ region (either $Gly^7$ or $Gly^{34}$) would have identical environments with respect to neighboring residues (see Figure 1). Thus, a total of only two cross-peaks would be anticipated, one corresponding to triple-helical conformation and one corresponding to monomeric conformation. Our results are consistent with this assumption.[2] Two sets of cross-peaks have been observed previously for Gly, Pro, and Hyp in (Pro-Hyp-Gly)$_{10}$ at 10 °C (*39*, *53*). One set of cross-peaks disappears above the melting temperature of (Pro-Hyp-Gly)$_{10}$ (*39*). The cross-peaks observed in our study can be assigned to a triple-helical or monomeric state (Table 1) on the basis of (a) the effect of temperature on the specific cross-peaks and (b) prior assignment of the proton resonances for Gly in (Pro-Hyp-Gly)$_{10}$ (*39*). One might believe that, if a lipidlike tail enhances the thermal stability of a triple helix, the region of the triple helix closest to the tail would be more stable than the region most distant from the tail. However, the HSQC data indicate that the $C_6$ tail enhances the stability of the entire triple-helical structure, as the spectra for the *N*-terminally labeled and *C*-terminally labeled peptide−amphiphiles are very similar. The equivalent spectral intensities of these two regions suggest that the presence of both triple-helical and monomeric resonances, even at low temperature, is most likely due to both triple-helical and monomeric species being present, as opposed to only a triple-helical species with less ordered regions (*39*).

The $^{15}$N-Gly residues used in this study appear to be sensitive probes of triple-helical conformation. NMR spectral behaviors of the effects of triple-helical conformation on Gly resonances are well documented (*55*, *56*). In addition, the upfield shift of monomeric Gly NH resonances as a function of temperature has been observed previously. $^{1}$H NMR

[2] The major cross-peak that corresponds to the monomeric conformation is often accompanied by a minor cross-peak (see Figures 2, 3, and 5). The presence of two monomeric cross-peaks suggests that, in the non-triple-helical state, the peptide−amphiphile has at least two distinct structures. Prior NMR studies have shown that the [IV-H1] sequence exists in several distinct structures when not in a triple-helical environment (*34*).

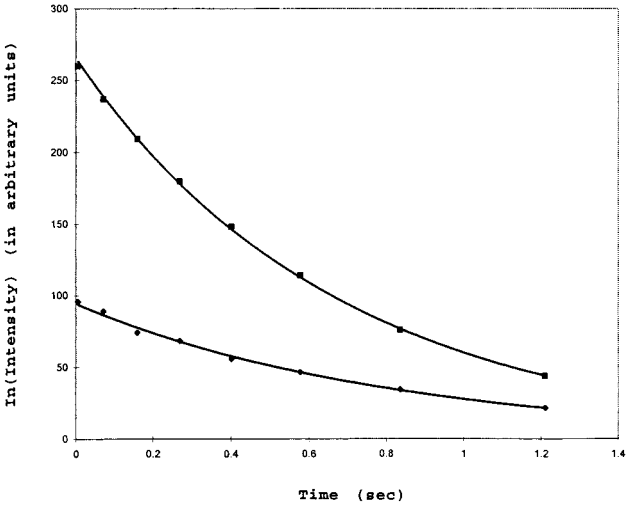


FIGURE 6: $^{15}$N $T_1$ relaxation decay curves for (■) trimeric and (◆) monomeric [$^{15}$N-$Gly^{34}$]-$C_6$-(Gly-Pro-Hyp)$_4$-[IV-H1]-(Gly-Pro-Hyp)$_4$ at 25 °C. The two sets of $T_1$ relaxation decay values generated could each be fit with a single exponential and $T_1$ values were calculated (see Table 2). Conditions are given in Experimental Procedures.

studies of the model peptide (Pro-Pro-Gly)$_{15}$ showed that as temperature increased, a weak Gly NH resonance at 8.1 ppm disappeared while the resonance at 7.85 ppm increased in intensity and shifted upfield (*57*). Solid-state $^{15}$N NMR indicated an upfield shift of 4.9 ppm for the Gly NH peak of (Pro-Pro-Gly)$_{10}$ upon decreased hydration and presumably decreased triple-helical stability (*58*). An upfield shift has been observed for the monomeric $^{1}$H resonances of [$^{15}N_2$-$Gly^6$,$Ala^{13}$]-T3-785 upon increasing temperature (*53*).

The intensities of the cross-peaks corresponding to triple helicity are different for the peptide and peptide−amphiphile. Since $C_6$-(Gly-Pro-Hyp)$_4$-[IV-H1]-(Gly-Pro-Hyp)$_4$ has a $T_m$ value of 42.2 °C (*10*), and thus forms a more thermally stable triple helix than the peptide alone (*8*), it is not surprising that the intensities of the triple-helical cross-peaks are stronger for the peptide−amphiphile. For collagenous peptides of low melting temperature, intensities are typically stronger for random coil resonances compared with triple-helical ones (*39*, *59*). While there is always some monomeric species present, the equilibrium toward triple helix appears to be more shifted in the peptide−amphiphile case. The relative intensities can be related to the $T_2$ relaxation decay values (*39*). These values are longer for the monomer than triple-helical species (see below), but the difference between the monomer and triple-helical values is comparable to that previously observed for the triple-helical peptide T3-785 (*39*).

*Dynamics of the Peptide−Amphiphile.* To study the internal dynamics of $C_6$-(Gly-Pro-Hyp)$_4$-[IV-H1]-(Gly-Pro-Hyp)$_4$, $^{15}$N relaxation data were acquired by using inverse-detected $^{1}$H−$^{15}$N NMR at 25 °C for the $^{15}$N-labeled peptide−amphiphiles described above.[3] The two sets of $T_1$ relaxation decay values generated for the $^{15}$N-$Gly^{34}$ peptide−amphiphile (Figure 6) could each be fit with a single exponential and $T_1$ values were calculated (Table 2). In similar fashion, the two sets of $T_1$ relaxation decay values generated for the $^{15}$N-$Gly^7$ peptide−amphiphile (data not shown) and the four sets

[3] Due to the weak NMR signals generated by the trimeric (Gly-Pro-Hyp)$_4$-[IV-H1]-(Gly-Pro-Hyp)$_4$ peptide, $^{15}$N relaxation data could not be obtained for this species.

Table 2: NMR Relaxation Parameters for $C_6$-(Gly-Pro-Hyp)$_4$-[IV-H1]-(Gly-Pro-Hyp)$_4$

| $^{15}$N-labeled residue | conformational state | $T_1$ (s) | $T_2$ (s) | NOE | $\tau_0$ (ns) | $\tau_i$ (ns) | $S_{NH}^2$ |
|---|---|---|---|---|---|---|---|
| Gly$^7$ | monomeric | 0.82 | 0.59 | −0.50 | 1.8 | 0.094 | 0.36 |
| Gly$^7$ | trimeric | 0.67 | 0.07 | 0.43 | 11.2 | 0.595 | 0.80 |
| Gly$^{19}$ | monomeric | 0.82 | 0.60 | −0.40 | 2.4 | 0.083 | 0.35 |
| Gly$^{19}$ | trimeric | 0.65 | 0.05 | 0.65 | 11.1 | 0.602 | 0.95 |
| Gly$^{19}$ | trimeric | 0.65 | 0.05 | 0.62 | 10.8 | 0.592 | 0.92 |
| Gly$^{19}$ | trimeric | 0.63 | 0.05 | 0.60 | 10.9 | 0.597 | 0.91 |
| Gly$^{34}$ | monomeric | 0.83 | 0.84 | −0.48 | 1.7 | 0.08 | 0.62 |
| Gly$^{34}$ | trimeric | 0.67 | 0.07 | 0.40 | 10.3 | 0.39 | 0.84 |

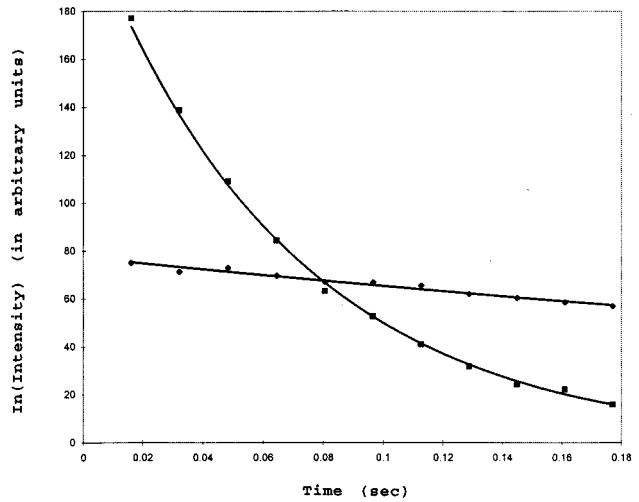


FIGURE 7: $^{15}$N $T_2$ relaxation decay curves for (■) trimeric and (◆) monomeric [$^{15}$N-Gly$^{34}$]-$C_6$-(Gly-Pro-Hyp)$_4$-[IV-H1]-(Gly-Pro-Hyp)$_4$ at 25 °C. The two sets of $T_2$ relaxation decay values generated could each be fit with a single exponential and $T_2$ values were calculated (see Table 2). Conditions are given in Experimental Procedures.

of $T_1$ relaxation decay values generated for the $^{15}$N-Gly$^{19}$ peptide−amphiphile (data not shown) could each be fit with a single exponential and $T_1$ values were calculated (Table 2). The two sets of $T_2$ relaxation decay values generated for the $^{15}$N-Gly$^{34}$ peptide−amphiphile (Figure 7) could each be fit with a single exponential and $T_2$ values were calculated (Table 2). In similar fashion, the two sets of $T_2$ relaxation decay values generated for the $^{15}$N-Gly$^7$ peptide−amphiphile (data not shown) and the four sets of $T_2$ relaxation decay values generated for the $^{15}$N-Gly$^{19}$ peptide−amphiphile (data not shown) could each be fit with a single exponential and $T_2$ values were calculated (Table 2). The heteronuclear NOE for each $^{15}$N-labeled species was also determined (Table 2).

The relaxation parameters for the monomeric peptide−amphiphile show striking differences from those for the triple-helical form (Table 2). The $T_1$ values for the monomer are longer than the $T_1$ values for the triple helix, regardless of which $^{15}$N-Gly is analyzed. The $T_2$ relaxation times for the monomeric species are approximately 10 times longer than the $T_2$ relaxation times for the trimeric conformation. The NOEs in the monomeric form are negative, while the trimeric form has large positive NOEs. These results are all consistent with those observed previously for triple-helical peptides. $T_1$ values were found to be longer for the random versus triple-helical state of the 36-residue collagenous peptide α1-CB2 (*59*). In similar fashion, the $T_1$ relaxation decay curve is slightly slower/longer for the monomeric state of T3-785 (*24*). The $T_2$ relaxation decay curve is also very long/slow for the monomeric state of T3-785 (*24*), with $T_2$ values of >100 ms for non-triple-helical species and 8 ms for the triple-helical form (*39*). For both T3-785 and T1-892 [which incorporates α1(I) residues 892−909], NOEs are negative for the monomer and positive for the trimer (*24*, *60*). Our results for the differences in dynamics parameters between the trimer and monomer state are in agreement with the dynamics studies of the collagenous peptide T3-785. This further confirms the assumptions made on the assignment of cross-peaks in the HSQC spectra for the two different conformational states.

For the trimer form, the $T_1$ and $T_2$ relaxation times and NOEs for the three $^{15}$N-Gly$^{19}$ residues are similar in magnitude (Table 2). The [IV-H1] region thus appears to be a well-formed triple helix.[4] In the trimer form, the $T_1$ and $T_2$ relaxation times and NOE value for the $^{15}$N-Gly$^7$ residue are similar to those for the $^{15}$N-Gly$^{34}$ residue (Table 2). These results indicate that the presence of the *N*-terminal $C_6$ tail does not significantly affect the conformational and dynamic properties of the adjacent (Gly-Pro-Hyp)$_4$ region.

$^1$H−$^{15}$N relaxation data were initially analyzed by the Lipari−Szabo model-free approach (*51*, *52*) as described in Experimental Procedures. $\tau_0$, $\tau_i$, and $S_{NH}^2$ values are listed in Table 2. The overall tumbling time for peptide monomer is about 5−10 times smaller than that for the peptide trimer. For all $^{15}$N-labeled positions within the peptide, average $\tau_0$ values are 2 ns for peptide monomer and 10.9 ns for peptide trimer. Upon comparison of these values with those reported by Daragan and Mayo (*50*) for the dependence of $\tau_0$ on the number of residues in a peptide, both $\tau_0$ values agree well with those expected for monomeric and trimeric species of the peptide−amphiphile. This information increases confidence in the assignment of peptide−amphiphile aggregation states.

Motional order parameters $S_{NH}^2$ (Table 2) indicate that the Gly N−H bond vector motions within the triple-helical peptide−amphiphile are rather restricted relative to those in the unfolded monomer. In the triple-helical state, $S_{NH}^2$ values for all Gly residues are greater than 0.8. In fact, for the three nonequivalent positions of Gly$^{19}$, $S_{NH}^2$ values are all above 0.9, indicating even greater motional restriction in the middle of the peptide sequence compared to nearer the termini, where $S_{NH}^2$ values were 0.8 and 0.84 for Gly$^7$ and Gly$^{34}$, respectively. It is possible that peptide−amphiphile end effects may be responsible for this behavior. At the *C*-terminal end, the Gly-Pro-Hyp region may slightly unwind (*55*), while the *N*-terminal end may be slightly misaligned due to the alkyl chains. However, it should be noted that the relaxation data obtained in this study apply to a fast time scale. Other studies have monitored backbone dynamics of triple-helical peptides on a slower time scale by measuring the hydrogen-exchange rates of individual amide protons (*24*, *60*). In those cases, the backbone motion of the triple helix was found to be quite different comparing the slow versus fast time scales.

Even though the Lipari−Szabo model-free approach (*51*, *52*) gives reasonable motional parameters, it was nonetheless

[4] The [IV-H1] region is based upon the gene-derived type IV collagen sequence, and therefore only Pro, but not Hyp, residues are present. Hydrogen bonds unique to Hyp residues are not essential for triple-helical stability within [IV-H1].

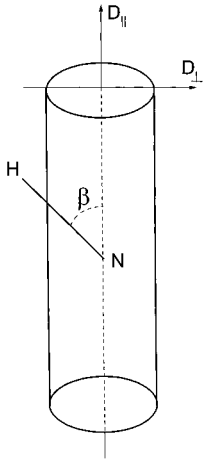


FIGURE 8: Model of the triple-helical peptide−amphiphile headgroup as a cylinder. The cylindrical triple helix has rotational diffusion coefficients $D_{||}$ and $D_{\perp}$ and an angle $\beta$ formed between the $D_{||}$ axis of rotation and the N−H bond vector.

originally formulated for molecules undergoing isotropic overall tumbling (see Experimental Procedures). Therefore, this model-free approach may not provide the most accurate picture of molecular dynamics in a collagen-based triple-helical peptide, which by its structural nature is more cylindrical than spherical in shape (*24*). The anisotropy of overall tumbling of a triple-helix "cylinder" prevents factorization of the correlation function as expressed in eq 2. The simplest motional model that considers the influence of rotational anisotropy is the model of rotational diffusion of a symmetric top.

For this analysis, model parameters are diffusion coefficients $D_{||}$ and $D_{\perp}$ and an angle $\beta$ formed between the $D_{||}$ rotational axis and an N−H bond vector. The triple helix is then simply considered a cylindrical molecule with $D_{||}$ running down the long axis (Figure 8). By use of eq 11, diffusion coefficients were calculated for each Gly N−H vector for different values of $\beta$. For visualization, the ratio $D_{||}/D_{\perp}$ was plotted versus the angle $\beta$ (Figure 9). $D_{||}/D_{\perp}$ values are more divergent at $\beta$ values below about 60°, but converge to 2.3 for $\beta$ between 60° and 90°. This indicates that these $^1$H−$^{15}$N relaxation data are best fit within these later limits. A value of $D_{||}/D_{\perp} = 2.3$ is consistent with the structural parameters of a triple helix wherein the helix dyad axis is defined by $D_{||}$. More interesting is the derived angle $\beta$. In a model triple helix, the angle which the Gly N−H bond actually makes with the helix dyad axis falls between 70° and 90° (*39*, *41*, *61*), clearly within the range derived for $\beta$ by using this motional model. This, in turn, strongly supports the idea that the structure of the acylated peptide is triple-helical.

Overall, the present study has indicated that the peptide headgroup of the $C_6$-(Gly-Pro-Hyp)$_4$-[IV-H1]-(Gly-Pro-Hyp)$_4$ peptide−amphiphile forms a continuous triple helix. The peptide−amphiphile triple-helical structure behaves similarly, in a dynamic sense, to a triple-helical peptide. The enhanced thermal stability of the peptide−amphiphile compared to analogous triple-helical peptides makes biochemical and biomaterial applications of this system most promising. In addition, peptide−amphiphiles are relatively simple to construct (*7*−*9*, *11*). Peptide−amphiphiles have already been demonstrated to enhance the promotion of cell adhesion and

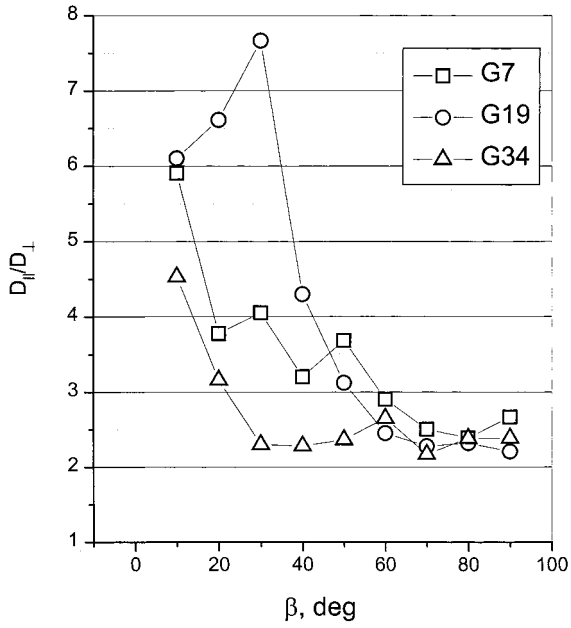


FIGURE 9: Plot of $D_{||}/D_{\perp}$ versus $\beta$ for trimeric (□) [$^{15}$N-Gly$^7$]-$C_6$-(Gly-Pro-Hyp)$_4$-[IV-H1]-(Gly-Pro-Hyp)$_4$, (○) [$^{15}$N-Gly$^{19}$]-$C_6$-(Gly-Pro-Hyp)$_4$-[IV-H1]-(Gly-Pro-Hyp)$_4$, and (△) [$^{15}$N-Gly$^{34}$]-$C_6$-(Gly-Pro-Hyp)$_4$-[IV-H1]-(Gly-Pro-Hyp)$_4$. By use of the motional model for anisotropic rotational diffusion of a symmetric top, parallel and perpendicular components of the rotational diffusion tensor, $D_{||}$ and $D_{\perp}$, respectively, were derived as discussed in Experimental Procedures. $D_{||}/D_{\perp}$ was then plotted versus the angle $\beta$. $D_{||}/D_{\perp}$ values for the three peptide−amphiphiles converge at $\beta = 60$−$90°$.

spreading on a variety of surfaces (*9*, *10*, *62*). With the multitude of organized structures formed by lipidlike compounds, peptide−amphiphiles could be utilized as targeted liposomes, sensors, receptors, or enzymes.

## REFERENCES

1. Stayton, P. S., Shimoboji, T., Long, C., Chilkoti, A., Chen, G., Harris, J. M., and Hoffman, A. S. (1995) *Nature 378*, 472−474.
2. Wesslén, B., Kober, M., Freij-Larsson, C., Ljungh, Å., and Paulsson, M. (1994) *Biomaterials 15*, 278−284.
3. Ozeki, E., and Matsuda, T. (1990) *ASAIO Trans. 36*, M294−M296.
4. Ito, Y., Kajihara, M., and Imanishi, Y. (1991) *J. Biomed. Mater. Res. 25*, 1325−1337.
5. Barrera, D. A., Zylstra, E., Lansbury, J. P. T., and Langer, R. (1993) *J. Am. Chem. Soc. 115*, 11010−11011.
6. Drumheller, P. D., Elbert, D. L., and Hubbell, J. A. (1994) *Biotechnol. Bioeng. 43*, 772−780.
7. Berndt, P., Fields, G. B., and Tirrell, M. (1995) *J. Am. Chem. Soc. 117*, 9515−9522.
8. Yu, Y. C., Berndt, P., Tirrell, M., and Fields, G. B. (1996) *J. Am. Chem. Soc. 118*, 12515−12520.
9. Yu, Y. C., Pakalns, T., Dori, Y., McCarthy, J. B., Tirrell, M., and Fields, G. B. (1997) *Methods Enzymol. 289*, 571−587.
10. Fields, G. B., Lauer, J. L., Dori, Y., Forns, P., Yu, Y.-C., and Tirrell, M. (1998) *Biopolymers 47*, 143−151.
11. Yu, Y.-C., Tirrell, M., and Fields, G. B. (1998) *J. Am. Chem. Soc. 120*, 9979−9987.
12. Macquaire, F., Baleux, F., Giaccobi, E., Huynh-Dinh, T., Neumann, J. M., and Sanson, A. (1992) *Biochemistry 31*, 2576−2580.
13. Cha, X., Ariga, K., and Kunitake, T. (1996) *Bull. Chem. Soc. Jpn. 69*, 163−167.
14. Brodsky, B., and Shah, N. K. (1995) *FASEB J. 9*, 1537−1546.
15. Fields, G. B. (1995) *Connect. Tissue Res. 31*, 235−243.
16. Grab, B., Miles, A. J., Furcht, L. T., and Fields, G. B. (1996) *J. Biol. Chem. 271*, 12234−12240.

17. Tanaka, T., Nishikawa, A., Tanaka, Y., Nakamura, H., Kodama, T., Imanishi, T., and Doi, T. (1996) *Protein Eng. 9*, 307−313.
18. Hojo, H., Akamatsu, Y., Yamauchi, K., Kinoshita, M., Miki, S., and Nakamura, Y. (1997) *Tetrahedron 53*, 14263−14274.
19. Tanaka, Y., Suzuki, K., and Tanaka, T. (1998) *J. Pep. Res. 51*, 413−419.
20. Ottl, J., Battistuta, R., Pieper, M., Tschesche, H., Bode, W., Kühn, K., and Moroder, L. (1996) *FEBS Lett. 398*, 31−36.
21. Goodman, M., Feng, Y., Melacini, G., and Taulane, J. P. (1996) *J. Am. Chem. Soc. 118*, 5156−5157.
22. Goodman, M., Melacini, G., and Feng, Y. (1996) *J. Am. Chem. Soc. 118*, 10928−10929.
23. Feng, Y., Melacini, G., and Goodman, M. (1997) *Biochemistry 36*, 8716−8724.
24. Fan, P., Li, M. H., Brodsky, B., and Baum, J. (1993) *Biochemistry 32*, 13299−13309.
25. Paterlini, M. G., Némethy, G., and Scheraga, H. A. (1995) *Biopolymers 35*, 607−619.
26. Fields, G. B. (1991) *J. Theor. Biol. 153*, 585−602.
27. Kühn, K., and Eble, J. (1994) *Trends Cell Biol. 4*, 256−261.
28. Morton, L. F., Peachey, A. R., Knight, C. G., Farndale, R. W., and Barnes, M. J. (1997) *J. Biol. Chem. 272*, 11044−11048.
29. Lauer, J. L., Gendron, C. M., and Fields, G. B. (1998) *Biochemistry 37*, 5279−5287.
30. Elomaa, O., Kangas, M., Sahlberg, C., Tuukkanen, J., Sormunen, R., Liakka, A., Thesleff, I., Kraal, G., and Tryggvason, K. (1995) *Cell 80*, 603−609.
31. Yamamoto, K., Nishimura, N., Doi, T., Imanishi, T., Kodama, T., Suzuki, K., and Tanaka, T. (1997) *FEBS Lett. 414*, 182−186.
32. Mielewczyk, S. S., Breslauer, K. J., Anachi, R. B., and Brodsky, B. (1996) *Biochemistry 35*, 11396−11402.
33. Chelberg, M. K., McCarthy, J. B., Skubitz, A. P. N., Furcht, L. T., and Tsilibary, E. C. (1990) *J. Cell Biol. 111*, 261−270.
34. Mayo, K. H., Parra-Diaz, D., McCarthy, J. B., and Chelberg, M. (1991) *Biochemistry 30*, 8251−8267.
35. Fields, C. G., Mickelson, D. J., Drake, S. L., McCarthy, J. B., and Fields, G. B. (1993) *J. Biol. Chem. 268*, 14153−14160.
36. Daragan, V. A., and Mayo, K. H. (1992) *J. Am. Chem. Soc. 114*, 4326−4331.
37. Daragan, V. A., Kloczewiak, M. A., and Mayo, K. H. (1993) *Biochemistry 32*, 10580−10590.
38. Daragan, V. A., Ilyina, E., and Mayo, K. H. (1993) *Biopolymers 33*, 521−533.
39. Li, M. H., Fan, P., Brodsky, B., and Baum, J. (1993) *Biochemistry 32*, 7377−7387.
40. Melacini, G., Feng, Y., and Goodman, M. (1996) *J. Am. Chem. Soc. 118*, 10725−10732.
41. Baum, J., and Brodsky, B. (1997) *Folding Des. 2*, R53−R60.
42. Melacini, G., Feng, Y., and Goodman, M. (1997) *Biochemistry 36*, 8725−8732.
43. Mayo, K. H. (1996) *Biopolymers (Pept. Sci.) 40*, 359−370.
44. Fields, C. G., Lloyd, D. H., Macdonald, R. L., Otteson, K. M., and Noble, R. L. (1991) *Pept. Res. 4*, 95−101.
45. Lauer, J. L., Fields, C. G., and Fields, G. B. (1995) *Lett. Pept. Sci. 1*, 197−205.
46. Fields, C. G., VanDrisse, V. L., and Fields, G. B. (1993) *Pept. Res. 6*, 39−47.
47. King, D. S., Fields, C. G., and Fields, G. B. (1990) *Int. J. Pept. Protein Res. 36*, 255−266.
48. Kay, L. E., Nicholson, L. K., Delaglio, F., Bax, A., and Torchia, D. A. (1992) *J. Magn. Reson. 97*, 359−375.
49. Kay, L. E., Torchia, D. A., and Bax, A. (1989) *Biochemistry 28*, 8972−8979.
50. Daragan, V. A., and Mayo, K. H. (1997) *Prog. NMR Spectrosc. 31*, 63−105.
51. Lipari, G., and Szabo, A. (1982) *J. Am. Chem. Soc. 104*, 4546−4559.
52. Lipari, G., and Szabo, A. (1982) *J. Am. Chem. Soc. 104*, 4559−4570.
53. Liu, X., Siegel, D. L., Fan, P., Brodsky, B., and Baum, J. (1996) *Biochemistry 35*, 4306−4313.
54. Balakrishnan, R., Siegel, D. L., Baum, J., and Brodsky, B. (1995) *FEBS Lett. 368*, 551−555.
55. Brodsky, B., Li, N. H., Long, C. G., Apigo, J., and Baum, J. (1992) *Biopolymers 32*, 447−451.
56. Long, C. G., Li, M. H., Baum, J., and Brodsky, B. (1992) *J. Mol. Biol. 225*, 1−4.
57. Kobayashi, Y., and Kyogoku, Y. (1973) *J. Mol. Biol. 81*, 337−347.
58. Naito, A., Tuzi, S., and Saito, H. (1994) *Eur. J. Biochem. 224*, 729−734.
59. Torchia, D. A., Lyerla, J. J. R., and Quattrone, A. J. (1975) *Biochemistry 14*, 887−900.
60. Liu, X., Kim, S., Dai, Q.-H., Brodsky, B., and Baum, J. (1998) *Biochemistry 37*, 15528−15533.
61. Fraser, R. D. B., MacRae, T. P., and Suzuki, E. (1979) *J. Mol. Biol. 129*, 463−481.
62. Winger, T. M., Ludovice, P. J., and Chaikof, E. L. (1996) *Biomaterials 17*, 437−440.

BI982315L